

Directed Polymer Transfer Matrices as a Unified Generator of Distinct One-Point Fluctuation Laws

Sen Mu,¹ Abbas Ali Saberi,^{2,1,*} Roderich Moessner,¹ and Mehran Kardar³

¹*Max Planck Institute for the Physics of Complex Systems, 01187 Dresden, Germany*

²*School of Science, Constructor University, Campus Ring 1, 28759 Bremen, Germany*

³*Department of Physics, Massachusetts Institute of Technology, Cambridge, USA*

(Dated: March 17, 2026)

We revisit the transfer-matrix approach to directed polymers in random media and show that a single ensemble of random transfer-matrix products provides a unified realization of the canonical one-point fluctuation laws in $(1+1)$ dimensions. For a fixed disorder realization, the polymer partition function is obtained as a contraction of the same product matrix $W(t)$, and different contractions reproduce the standard KPZ subclasses: Tracy–Widom GUE (point-to-point), GOE (point-to-line), GSE (half-space point-to-point), and Baik–Rains (stationary line-to-point). In each case, we observe $t^{1/3}$ free-energy fluctuation growth and convergence of standardized distributions with low-order cumulants close to the corresponding universal benchmarks. Viewing geometry-dependent subclasses as projections of a single matrix-product ensemble naturally suggests additional observables intrinsic to $W(t)$. As an example, we examine the leading eigenvalue $\lambda_1(t)$ whose logarithm exhibits $t^{1/3}$ scaling, while its standardized statistics remain distinct from the canonical Tracy–Widom laws within the accessible range. This transfer-matrix perspective thus organizes known KPZ one-point subclasses within a finite-dimensional matrix framework and highlights matrix-level fluctuation observables beyond geometry-selected universality classes.

I. INTRODUCTION

The Kardar-Parisi-Zhang (KPZ) universality class governs a broad range of non-equilibrium fluctuation phenomena in one spatial dimension, including stochastic interface growth, interacting particle systems, and directed polymers in random media (DPRM) [1–5]. Beyond model-specific details, KPZ systems share a characteristic scaling structure: For growing interfaces, typical height fluctuations initially grow in time as t^β with $\beta = 1/3$, spatial correlations spread as $t^{1/z}$ with dynamic exponent $z = 3/2$, ultimately saturating at finite size with roughness exponent $\alpha = \beta z$ [1–3, 5]. An equivalent formulation of the same universality class is provided by directed polymers in random media (DPRM), in which one studies a directed path propagating through a quenched random energy landscape; the logarithm of its partition function defines a free energy whose fluctuations obey the same $t^{1/3}$ scaling, while the transverse wandering of the polymer endpoint scales as $t^{2/3}$.

A central insight of the modern theory is that KPZ universality in $1+1$ dimensions contains distinct one-point fluctuation subclasses, selected by geometry and boundary conditions (or, for full-line growth, by initial data) [4–7]. For curved (droplet) geometry, the properly centered and scaled height/free-energy fluctuations converge to the Tracy-Widom GUE distribution [8–11]. For flat geometry, the limiting law is Tracy-Widom GOE [6, 12]. For stationary geometry, obtained by imposing a two-sided Brownian initial profile, the limiting one-point law is the Baik-Rains distribution [6, 7]. In half-space set-

tings, the presence of a boundary introduces additional subclasses; in particular, at the appropriate boundary condition, one obtains Tracy-Widom GSE fluctuations [12–14]. Different KPZ subclasses can compete and lead to crossovers when distinct growth sectors are coupled, as shown for growth on crossing substrates with various subclass pairings [15]. These results provide one of the clearest examples of universal fluctuation laws controlled by geometry rather than microscopic dynamics.

Traditionally, these subclasses are realized through distinct dynamical settings: different initial data, boundary geometries, or half-space constructions are imposed at the level of the growth process itself. In this sense, the canonical one-point laws appear as outcomes of separate evolutions, each tailored to a particular geometry.

The directed polymer formulation is historically one of the foundational routes into KPZ physics. In the lattice DPRM, the partition function is obtained by summing Boltzmann weights over all directed paths through a quenched random energy landscape, and its logarithm encodes the polymer free energy [2–4, 16]. The overall sum can be computed recursively in polynomial time with a transfer-matrix algorithm, in which the sum vector at time t is updated from time $t-1$ by multiplication with a random near-diagonal matrix. This formulation played a central role in early analytical treatments and numerical studies of DPRM/KPZ systems, because it makes the growth recursion explicit and gives direct access to finite-time fluctuation statistics [2, 16, 17]. At the same time, it naturally presents a matrix-product viewpoint that suggests connecting polymer observables to matrix elements and spectral statistics.

The connection between KPZ physics and random matrix theory (RMT) is now a cornerstone of the field. The appearance of Tracy-Widom laws in KPZ fluctu-

* asaberi@constructor.university

ations was first understood through exact solutions of integrable growth models and exclusion processes, and through their mapping to determinantal/Pfaffian structures [6–8]. In this correspondence, the edge fluctuations of random matrices provide the universal limiting distributions (GUE, GOE, GSE), while KPZ models provide the dynamical physical realization [4, 5, 9, 12]. Subsequent exact solutions of the continuum KPZ equation and continuum directed polymer further cemented this link, showing explicitly how the one-point free-energy distribution crosses over to the Tracy–Widom laws in the long-time limit [10, 11].

In the present work, we revisit the transfer-matrix formulation of lattice DPRM and adopt a complementary viewpoint. Rather than treating each KPZ subclass as arising from a separate dynamical construction, we regard the time-ordered product of random transfer matrices

$$W(t) = T(t)T(t-1) \cdots T(1)$$

as the fundamental object. For a fixed disorder realization, the polymer partition function is a matrix element of this product. We show numerically that different boundary contractions of the same random matrix product $W(t)$ reproduce the canonical one-point KPZ subclasses: point-to-point (droplet) yields Tracy–Widom GUE, point-to-line (flat) yields Tracy–Widom GOE, a stationary line-to-point construction yields Baik–Rains, and a half-space implementation with an absorbing boundary yields Tracy–Widom GSE. In all cases, we recover the expected $t^{1/3}$ fluctuation growth and observe agreement of standardized distributions and low-order cumulants with the corresponding universal benchmarks.

This matrix-product perspective organizes geometry-dependent KPZ subclasses as distinct projections of a single finite-dimensional random-matrix ensemble. In this sense, the well-known Tracy–Widom and Baik–Rains fluctuation laws arise from different contractions of the same object, rather than from fundamentally distinct stochastic evolutions.

At the same time, the transfer-matrix ensemble naturally contains observables that are not tied to canonical endpoint geometries. Beyond matrix elements, one may examine intrinsic spectral properties of $W(t)$, such as its leading eigenvalue. Motivated by the central role played by the edge eigenvalue in classical random matrix theory, we consider the growth of $\ln \lambda_1(t)$, where $\lambda_1(t)$ is the largest eigenvalue of $W(t)$. While $\ln \lambda_1(t)$ exhibits KPZ-like $t^{1/3}$ fluctuation growth over an intermediate time window, its standardized one-point distribution and low-order cumulants remain distinct from the canonical Tracy–Widom benchmarks within the numerically accessible regime. This suggests that the transfer-matrix ensemble may encode additional fluctuation structures beyond the geometry-selected KPZ subclasses.

The remainder of the paper is organized as follows. In Sec. II we introduce the lattice directed-polymer transfer-matrix formulation and define the ran-

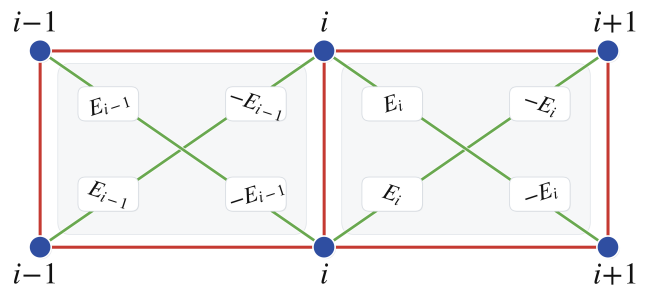


FIG. 1. Illustration of the random energies on the green bonds in the 6-vertex model representation considered for the directed polymer in random media.

dom matrix-product ensemble studied here. In Sec. III we show how different contractions of the same product matrix realize the canonical one-point KPZ subclasses and present numerical evidence for Tracy–Widom GUE, GOE, and GSE statistics, as well as Baik–Rains fluctuations in the stationary construction. In Sec. IV we turn to matrix-level observables beyond endpoint free energies, focusing in particular on the largest eigenvalue of the transfer-matrix product. Finally, in Sec. V we summarize the results and discuss future directions from the spectral perspective opened by this framework.

II. DIRECTED POLYMER IN RANDOM MEDIA AND TRANSFER-MATRIX FORMULATION

We consider directed polymers in random media (DPRM), where the central object is the partition function obtained by summing over all directed paths connecting specified initial and final points. For a polymer starting at $(x_0, 0)$ and ending at (x, t) , with $x_0, x \in [1, \dots, N]$ and $t > 0$, the partition function is defined as

$$Z(x, x_0, t) = \sum_{\text{directed paths}} \exp \left[- \sum_{\alpha=1}^t E_{x, x_0}^\alpha \right]. \quad (1)$$

Here, $\sum_{\alpha=1}^t E_{x, x_0}^\alpha$ denotes the total random energy accumulated along each path, and the Boltzmann weight assigns larger statistical weight to lower-energy paths. The associated free energy is

$$F(x, x_0, t) = - \ln Z(x, x_0, t). \quad (2)$$

A convenient way to evaluate the partition function is through a transfer-matrix formulation, which takes advantage of the directed nature of the paths. Denoting by $T(t)$ the transfer matrix at time slice t , the partition function satisfies the recursion relation

$$Z(x, x_0, t) = \sum_{x'} \langle x | T(t) | x' \rangle Z(x', x_0, t-1). \quad (3)$$

It is therefore useful to introduce the ordered product of

transfer matrices

$$W(t) = \prod_{t'=1}^t T(t'), \quad (4)$$

so that the partition function can be written compactly as the matrix element

$$Z(x, x_0, t) = \langle x | W(t) | x_0 \rangle. \quad (5)$$

Equation (5) makes clear that all polymer observables considered in this work are matrix elements—or contractions—of the same random matrix product $W(t)$. For a fixed realization of disorder, the entire geometry dependence of the polymer free energy is encoded in how this product matrix is contracted with boundary vectors.

In this work, we adapt a specific realization of DPRM motivated by a 6-vertex model in a random environment. As depicted in Fig. 1, random energies are assigned to diagonal bonds of the model in a manner that leads to a particularly simple local transfer matrix. We adopt this choice because it provides an efficient and transparent transfer-matrix representation, while preserving the essential ingredients of the problem. The corresponding tridiagonal transfer matrix at each time slice now takes the form

$$T(t') = \begin{pmatrix} M_{11}^{t'} & 1 & 0 & 0 & \cdots \\ 1 & M_{22}^{t'} & 1 & 0 & \cdots \\ 0 & 1 & M_{33}^{t'} & 1 & \cdots \\ 0 & 0 & 1 & M_{44}^{t'} & \cdots \\ \vdots & \vdots & \vdots & \vdots & \ddots \end{pmatrix}, \quad (6)$$

with time-dependent diagonal entries

$$M_{ii}^{t'} = e^{-2E_{i-1}^{t'}} + e^{2E_i^{t'}}. \quad (7)$$

The random variables $E_i^{t'}$ are the (diagonal) bond energies of the corresponding vertex model (Fig. 1) taken to be independent and identically distributed random variables drawn from a uniform distribution with mean μ and standard deviation σ ,

$$E_i^{t'} \in [\mu - \sqrt{3}\sigma, \mu + \sqrt{3}\sigma]. \quad (8)$$

At the boundaries, the diagonal entries of the transfer matrix are modified according to the vertex-model geometry. In particular, we impose

$$M_{11}^{t'} = e^{-2E_0^{t'}} + e^{2E_1^{t'}}, \quad M_{NN}^{t'} = e^{-2E_{N-1}^{t'}}. \quad (9)$$

These boundary terms complete the definition of the DPRM transfer-matrix ensemble considered in this work.

Throughout this work, we focus on system sizes N and evolution times t chosen so as to probe the pre-saturation regime of KPZ scaling. For $1 \ll t \ll N^{3/2}$, finite-size effects are subdominant and free-energy fluctuations are expected to exhibit the characteristic $t^{1/3}$ growth associated with KPZ universality. The numerical results presented below are obtained within this scaling window.

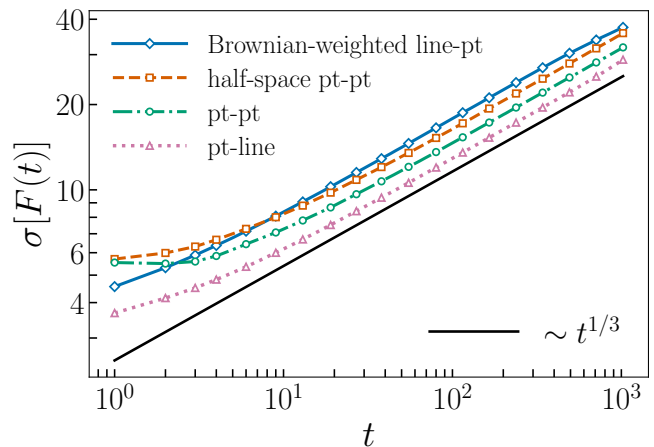


FIG. 2. Standard deviation of the free energy, $\sigma[F(t)]$, as a function of time t for the Brownian-weighted line-to-point, half-space point-to-point, point-to-point, and point-to-line boundary conditions, plotted on log-log scales. The black solid line indicates the power law $t^{1/3}$. The data are consistent with KPZ scaling of the free-energy fluctuations in all four cases. Model parameters are $N = 128$, $\mu = 0$, and $\sigma = 3$, with evolution up to $t = 1024$ over 10^6 disorder realizations.

III. KPZ SUBUNIVERSALITY FROM PRODUCT MATRIX ELEMENTS

It is well established that, for DPRM in $1 + 1$ dimensions, different choices of endpoint geometry, and boundary data select distinct one-point KPZ fluctuation subclasses. In the conventional formulation, these subclasses are realized by modifying the geometry or initial condition of the growth process itself.

In the transfer-matrix framework developed here, the situation can be viewed differently. For a fixed disorder realization, the entire evolution is encoded in the single product matrix $W(t)$. Geometry then enters only through how this matrix is contracted with boundary vectors. Different one-point KPZ subclasses, therefore, correspond to different contractions of the same random matrix product.

In particular, fixing both the starting point and the endpoint realizes the droplet geometry, for which the centered and scaled free energy is expected to approach the Tracy–Widom GUE distribution. Summing uniformly over one endpoint while keeping the other fixed corresponds to the flat geometry and leads to the Tracy–Widom GOE distribution. For the stationary subclass, the corresponding one-point law is the Baik–Rains distribution, which is associated with a stationary free-energy profile and is canonically realized by a two-sided Brownian profile in the continuum setting. In half-space settings, the presence of a boundary introduces an additional subclass structure; in the absorbing-wall realization considered below, the resulting point-to-point free-energy fluctuations are naturally compared with the

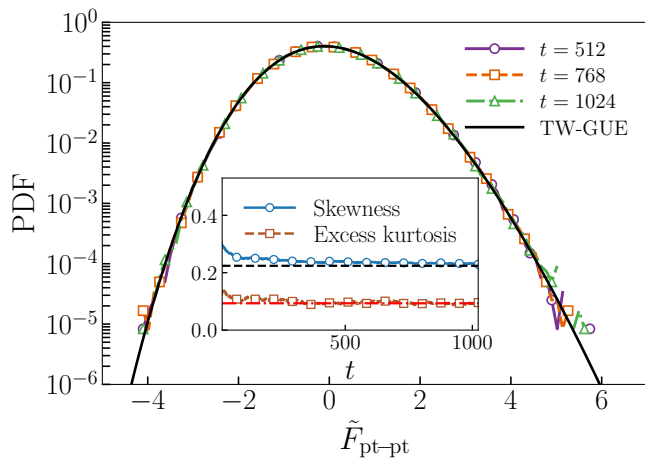


FIG. 3. Statistics of the standardized free energy for the point-to-point boundary condition. Main: Distribution of the standardized free energy $\tilde{F}_{\text{pt-pt}}$ at different times ($t = 512, 768, 1024$), together with the standardized TW-GUE distribution. Inset: Time evolution of the skewness and excess kurtosis of the standardized free energy. The black dashed and red dot-dashed lines denote the corresponding TW-GUE values, 0.22 and 0.09, respectively. Model parameters are $N = 128$, $\mu = 0$, $\sigma = 3$, and $x_0 = 64$ with evolution up to $t = 1024$ over 10^6 disorder realizations.

Tracy–Widom GSE distribution.

In all of these subclasses, we characterize the fluctuations of the free energy through its standard deviation

$$\sigma[F(t)] = \sqrt{\langle F(t)^2 \rangle - \langle F(t) \rangle^2}, \quad (10)$$

where $\langle \dots \rangle$ denotes the disorder average. As shown in Fig. 2, we find that $\sigma[F(t)]$ exhibits a clear power-law growth in time in all four cases shown, consistent with the KPZ scaling form $\sigma[F(t)] \sim t^{1/3}$.

In the following, we present the full distributions of the standardized free energy,

$$\tilde{F}(t) = -(F(t) - \langle F(t) \rangle) / \sigma[F(t)], \quad (11)$$

for each of these subclasses and compare them with the corresponding universal benchmark distributions.

A. Tracy-Widom GUE and GOE distributions

We first consider two basic contractions of the product matrix $W(t)$ corresponding to fixed and partially summed endpoints:

$$\begin{cases} F_{\text{pt-pt}}(t) = -\ln \langle x_0 | W(t) | x_0 \rangle, & \text{for point-to-point,} \\ F_{\text{pt-line}}(t) = -\ln \sum_x \langle x | W(t) | x_0 \rangle, & \text{for point-to-line,} \end{cases} \quad (12)$$

with fixed x_0 . In the first case, both endpoints are fixed, while in the second case, the final endpoint is summed uniformly over all transverse positions. These two contractions are expected to probe the droplet (TW-GUE) and flat (TW-GOE) subclasses, respectively.

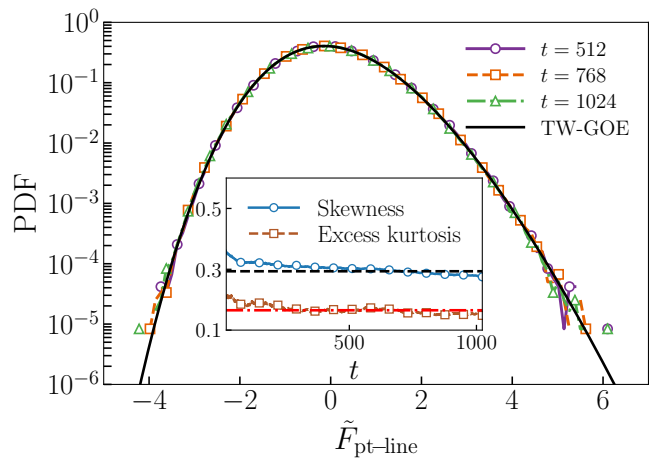


FIG. 4. Statistics of the standardized free energy for the point-to-line boundary condition. Main: Distribution of the standardized free energy $\tilde{F}_{\text{pt-line}}$ at different times ($t = 512, 768, 1024$), together with the standardized TW-GOE distribution. Inset: Time evolution of the skewness and excess kurtosis of the standardized free energy. The black dashed and red dot-dashed lines denote the corresponding TW-GOE values, 0.29 and 0.17, respectively. Model parameters are $N = 128$, $\mu = 0$, $\sigma = 3$ and $x_0 = 64$ with evolution up to $t = 1024$ over 10^6 disorder realizations.

We present the free-energy statistics for the point-to-point boundary condition in Fig. 3. The standardized distribution at late time is well described by the Tracy–Widom GUE benchmark. This identification is further supported by the time evolution of the skewness and excess kurtosis, which approach the corresponding TW-GUE values within the accessible time range.

We next present the free-energy statistics for the point-to-line boundary condition in Fig. 4. In this case the standardized distribution is well described by the Tracy–Widom GOE benchmark, as expected for the flat subclass. This identification is again supported by the corresponding skewness and excess kurtosis, which evolve toward the TW-GOE values at late times.

B. Tracy-Widom GSE distribution

We next modify the contraction by introducing a boundary constraint that effectively restricts the polymer to a half-space. Within the transfer-matrix framework, this corresponds to altering the structure of $W(t)$ near the boundary while keeping the bulk disorder ensemble unchanged.

The half space is realized by placing an absorbing wall at the boundary, taken to be the last site $x = N$ in our model, and by choosing the polymer to start and end at the adjacent site $x_0 = N - 1$. An absorbing wall means that any polymer trajectory that reaches $x = N$ is terminated and contributes no further weight. Equivalently, the wall site cannot serve as the starting point of any fur-

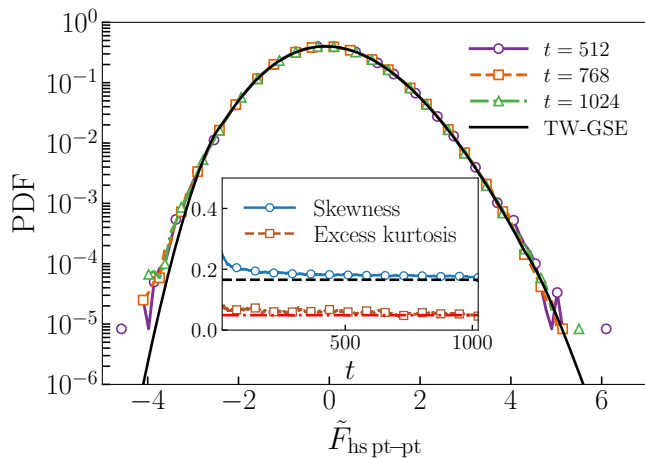


FIG. 5. Statistics of the standardized free energy for the point-to-point boundary condition in half space. Main: Distribution of the standardized free energy $\tilde{F}_{\text{hs pt-pt}}$ at different times ($t = 512, 768, 1024$), together with the standardized TW-GSE distribution. Inset: Time evolution of the skewness and excess kurtosis of the standardized free energy. The black dashed and red dot-dashed lines denote the corresponding TW-GSE values, 0.16 and 0.04, respectively. Model parameters are $N = 128$, $\mu = 0$, $\sigma = 3$ and $x_0 = 127$ with evolution up to $t = 1024$ over 10^6 disorder realizations.

ther continuation of the polymer. In our transfer-matrix formulation, this condition can be imposed at each step by

$$\forall x', t' : \quad \langle x' | T(t') | N \rangle = 0, \quad (13)$$

so that no propagation proceeds outward from the absorbing site. With this boundary condition, the half-space point-to-point free energy is defined by

$$F_{\text{hs pt-pt}}(t) = -\ln \langle x_0 | W(t) | x_0 \rangle, \quad (14)$$

with $x_0 = N - 1$ and the absorbing-wall condition in Eq. (13).

A convenient implementation keeps the wall site as an auxiliary absorbing state. The polymer is then allowed to enter $x = N$ from $x = N - 1$, but it cannot return. At the level of each one-step transfer matrix $T(t')$, this corresponds to choosing the block acting on the last two sites $\{|N - 1\rangle, |N\rangle\}$ to be triangular,

$$T_{\{|N-1, N\}}(t') = \begin{pmatrix} M_{N-1}^{t'} & 0 \\ 1 & M_N^{t'} \end{pmatrix}, \quad (15)$$

which permits transitions $N - 1 \rightarrow N$ while forbidding transitions $N \rightarrow N - 1$. For the point-to-point matrix element $\langle x_0 | W(t) | x_0 \rangle$, this construction removes contributions from trajectories that ever reach the absorbing site and is therefore equivalent for the observable considered here.

The resulting free-energy statistics are shown in Fig. 5. We find that the standardized free-energy distribution

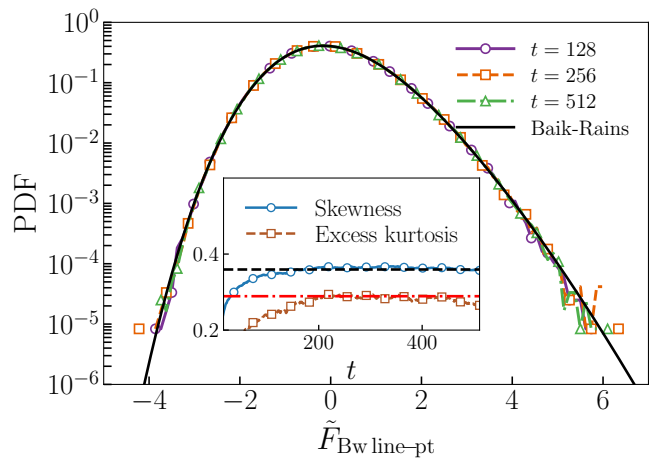


FIG. 6. Statistics of the standardized free energy for the Brownian weighted line-to-point boundary condition. Main: Distribution of the standardized free energy $\tilde{F}_{\text{Bw line-pt}}$ at different times ($t = 128, 256, 512$), together with the standardized Baik-Rains distribution. Inset: Time evolution of the skewness and excess kurtosis of the standardized free energy. The black dashed and red dot-dashed lines denote the corresponding Baik-Rains values, 0.36 and 0.29, respectively. Model parameters are $N = 128$, $\mu = 0$, $\sigma = 3$, $x_0 = 64$ and $\sigma_B = 6.2$ with evolution up to $t = 512$ over 10^6 disorder realizations.

is well described by the Tracy–Widom GSE benchmark. This identification is further supported by the time evolution of the skewness and excess kurtosis, which move toward the corresponding TW-GSE values at late times.

C. Baik-Rains distribution

We now turn to a construction aimed at probing the stationary KPZ subclass within the same transfer-matrix framework. In the continuum formulation, the stationary subclass is obtained by initializing the interface with a two-sided Brownian profile. Under time evolution, such a profile preserves stationarity of height increments, and the resulting one-point fluctuations converge to the Baik–Rains distribution.

To approximate this setting in the present discrete transfer-matrix formulation, we introduce a Brownian-weighted initial vector $|u\rangle$ with components

$$u(x) = e^{B(x)}, \quad (16)$$

where $B(x)$ is a discrete two-sided random walk referenced to a central site and fixed by the convention $B(x_{\text{mid}}) = 0$. This removes an arbitrary additive constant and defines a random initial free-energy profile. The corresponding free energy is obtained from the con-

traction

$$\begin{aligned} F_{\text{Bw line-pt}}(t) &= -\ln \sum_x e^{B(x)} \langle x_0 | W(t) | x \rangle \\ &= -\ln \langle x_0 | W(t) | u \rangle, \end{aligned} \quad (17)$$

which represents a Brownian-weighted line-to-point observable from the same product matrix $W(t)$. In other words, the stationary-type boundary condition is implemented by summing over all starting positions with random initial weights $e^{B(x)}$, while keeping the bulk disorder ensemble unchanged. After centering and rescaling, the resulting one-point free-energy distribution is then compared with the Baik–Rains benchmark.

In the discrete transfer-matrix realization considered here, the exact stationary measure of the microscopic dynamics is not known analytically and may depend on the disorder distribution as well as on the update rule. We therefore treat the standard deviation parameter σ_B of the Brownian increments as an effective tuning parameter. Specifically, we determine σ_B empirically by requiring that the late-time skewness and excess kurtosis of the standardized free-energy fluctuations approach the Baik–Rains benchmark values as closely as possible within the accessible time window.

It is important to emphasize that this Brownian-weighted initialization should be viewed as an effective approximation to the stationary subclass rather than an exact invariant measure of the discrete dynamics. Finite-size and finite-time corrections can affect one-point and two-point observables differently, and the optimal value of σ_B for matching one-point cumulants need not coincide with that inferred from spatial roughness diagnostics. Within the present system sizes and evolution times, we therefore focus on one-point fluctuation statistics as the primary diagnostic of the stationary subclass.

The numerical results are shown in Fig. 6. After centering and rescaling, the one-point free-energy distribution exhibits good agreement with the Baik–Rains benchmark over the accessible time range, and the low-order cumulants approach the expected universal values. This indicates that, within the unified transfer-matrix ensemble, the stationary KPZ subclass can be effectively realized through a Brownian-weighted contraction of the same product matrix $W(t)$.

IV. MATRIX-LEVEL OBSERVABLES BEYOND ENDPPOINT GEOMETRIES

The contractions considered in Sec. III probe DPRM free energies associated with specific endpoint geometries. However, the transfer-matrix product $W(t)$ contains more information than its matrix elements alone. It is therefore natural to ask whether intrinsic matrix-level observables, independent of canonical boundary geometries, also exhibit KPZ-like fluctuation behavior. In this section, we focus on one such observable: the largest eigenvalue of the product matrix $W(t)$.

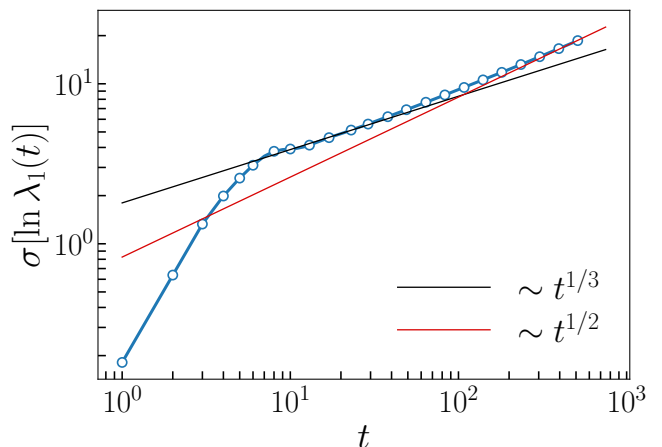


FIG. 7. Standard deviation of the logarithmic leading eigenvalue, $\sigma[\ln \lambda_1(t)]$, as a function of time t on log-log scales. The solid guide lines indicate the power laws $t^{1/3}$ (black) and $t^{1/2}$ (red). The data display an intermediate regime compatible with KPZ-like $t^{1/3}$ growth, followed at later times by a crossover toward a steeper scaling. Model parameters are $N = 128$, $\mu = 0$ and $\sigma = 3$ with evolution up to $t = 512$ over 10^6 disorder realizations.

A. Largest Eigenvalue

Let $\{\lambda_i(t)\}_{i=1}^N$ denote the eigenvalues of the product matrix $W(t)$, ordered by decreasing modulus,

$$|\lambda_1(t)| \geq |\lambda_2(t)| \geq \dots \geq |\lambda_N(t)|. \quad (18)$$

Since each transfer matrix has strictly positive entries, the product $W(t)$ is also strictly positive. By the Perron–Frobenius theorem, the leading eigenvalue $\lambda_1(t)$ is therefore real and positive. This makes

$$F_1(t) = \ln \lambda_1(t) \quad (19)$$

a natural spectral growth observable to study.

Unlike the canonical point-to-point or point-to-line free energies, $\ln \lambda_1(t)$ is not associated with a specific endpoint geometry. It therefore provides an example of a matrix-level observable intrinsic to the ensemble defined by $W(t)$. To assess whether $\ln \lambda_1(t)$ displays KPZ-like behavior, we examine the growth of its fluctuations. Over an intermediate time window, we observe that the standard deviation grows approximately as

$$\sigma[\ln \lambda_1(t)] \sim t^{1/3}. \quad (20)$$

consistent with KPZ scaling, as shown in Fig. 7. This scaling regime is restricted in time and limited by finite- N effects; beyond a crossover scale, deviations become visible.

We also examine the full distribution of the standardized $\ln \lambda_1(t)$ at different times and compute its skewness and excess kurtosis, presented in Fig. 8. Within the accessible time range, these cumulants remain systematically distinct from the canonical Tracy–Widom GUE and

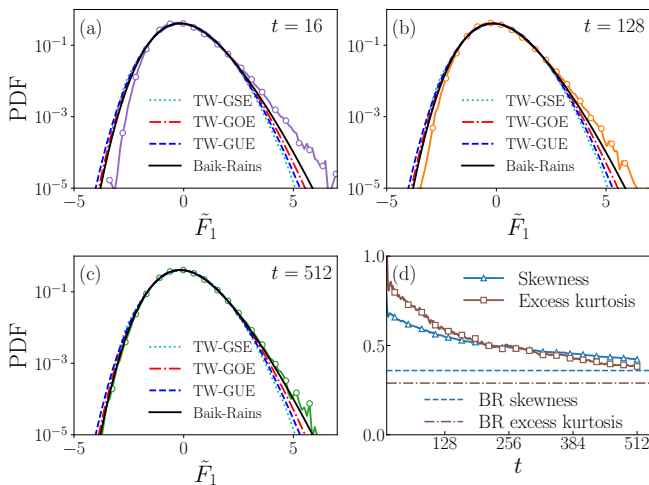


FIG. 8. Statistics of the standardized logarithmic leading eigenvalue $\tilde{F}_1(t)$. Panels (a)–(c) show the distribution of $\tilde{F}_1(t)$ at times $t = 16, 128, 512$, compared with the standardized TW-GSE, TW-GOE, TW-GUE, and Baik–Rains benchmark distributions. Panel (d) shows the time evolution of the skewness and excess kurtosis of $\tilde{F}_1(t)$. The horizontal dashed and dot-dashed lines indicate the Baik–Rains skewness and excess kurtosis, respectively, shown only as reference values for comparison. Among these canonical laws, Baik–Rains provides the closest overall reference to the numerical data over the accessible range and is therefore included as a guide to the eye, rather than as an identified limiting law. Model parameters are $N = 128$, $\mu = 0$, and $\sigma = 3$, with evolution up to $t = 512$ over 10^6 disorder realizations.

GOE benchmark values. In particular, no clear convergence toward known TW cumulants is observed over the simulated regime.

Taken together, these results indicate that $\ln \lambda_1(t)$ exhibits KPZ-like $t^{1/3}$ fluctuation growth over an intermediate window, while its one-point statistics do not coincide with geometry-selected Tracy–Widom or Baik–Rains subclasses discussed in Sec. III.

B. Spectral Perspective

The leading eigenvalue provides only the simplest example of an intrinsic matrix-level observable. More generally, the full spectrum of $W(t)$ encodes information about the structure of the random matrix product associated with DPRM evolution. In contrast to the endpoint free energies, which are selected by specific boundary contractions, spectral observables are determined by the internal structure of $W(t)$ itself. The transfer-matrix viewpoint, therefore, suggests a broader class of fluctuation observables derived from the same disorder ensemble. While the present work focuses on the largest eigenvalue as a representative, a systematic study of the spectral statistics of $W(t)$ is desirable, but lies beyond the scope of this paper.

V. DISCUSSION AND OUTLOOK

We have shown that a single lattice DPRM transfer-matrix ensemble provides a compact realization of the canonical $(1 + 1)$ -dimensional KPZ one-point subclass structure. The central object is the random product matrix $W(t) = T(t)T(t-1)\cdots T(1)$, from which polymer partition sums and free energies are obtained by boundary contraction. Within this framework, geometry does not require distinct stochastic evolutions; instead, it is encoded algebraically through different contractions of the same random matrix product. Point-to-point, point-to-line, stationary, and half-space settings are realized by varying only the boundary vectors or endpoint summations while keeping the bulk disorder ensemble fixed.

For the canonical endpoint observables, our numerics reproduce the expected $t^{1/3}$ free-energy fluctuation scaling and yield one-point distributions that are in good agreement with the corresponding universal benchmarks. The droplet and flat contractions approach Tracy–Widom GUE and GOE, respectively; the half-space construction yields behavior consistent with Tracy–Widom GSE; and a Brownian-weighted contraction provides an effective realization of the Baik–Rains stationary subclass. Taken together, these results show that geometry-dependent KPZ one-point subclasses can be organized directly at the level of a finite-dimensional matrix-product ensemble.

Beyond these canonical projections, the transfer-matrix product $W(t)$ naturally gives access to intrinsic matrix-level observables. As a representative example, we examined the logarithm of the leading eigenvalue $\ln \lambda_1(t)$; within the numerically accessible regime, this spectral observable exhibits KPZ-like $t^{1/3}$ fluctuation growth over an intermediate time window. At the same time, its standardized distribution and cumulants remain distinct from the known Tracy–Widom and Baik–Rains subclasses over the simulated range. Thus, while the present results do not establish an asymptotic limiting law for this observable, they indicate that the unified transfer-matrix ensemble contains fluctuation structures not directly tied to the standard geometry-selected subclasses.

This perspective suggests a broader interpretation of the KPZ one-point structure. The familiar Tracy–Widom and Baik–Rains laws arise as specific projections of a larger random matrix product. In this sense, geometry selects particular observables of $W(t)$, rather than defining fundamentally different stochastic processes. The transfer-matrix formulation, therefore, provides a compact framework in which canonical KPZ subclasses coexist with additional matrix-derived observables whose statistical properties remain to be explored.

Several directions follow naturally from the present viewpoint. On the numerical side, larger system sizes and longer times would clarify the intrinsic spectral observables such as $\ln \lambda_1(t)$. On the conceptual side, it would be interesting to understand more systematically how spec-

tral observables of $W(t)$ relate to the other DPRM configurations, and whether additional matrix-level quantities admit universal descriptions. More broadly, the transfer-matrix approach opens a route to studying DPRM and KPZ fluctuations through structured random matrix products, complementing integrable and continuum formulations.

In summary, a single ensemble of finite-dimensional DPRM transfer-matrix products provides a unified framework for the canonical geometry-dependent KPZ one-point fluctuation laws, while simultaneously suggest-

ing a wider class of matrix-level observables whose scaling properties extend beyond the canonical Tracy–Widom subclasses.

Acknowledgements. S.M. thanks Jonas Karcher for helpful discussions. This work was funded by the Deutsche Forschungsgemeinschaft (DFG, German Research Foundation) under Project No. 557852701 (A.A.S.). The study was also supported by the Advanced Study Group “Strongly Correlated Extreme Fluctuations” at the Max Planck Institute for the Physics of Complex Systems, Dresden (2024/25) [18], and the NSF through Grant No. DMR-2218849 (M.K.).

-
- [1] M. Kardar, G. Parisi, and Y.-C. Zhang, Dynamic scaling of growing interfaces, *Physical Review Letters* **56**, 889 (1986).
- [2] T. Halpin-Healy and Y.-C. Zhang, Kinetic roughening phenomena, stochastic growth, directed polymers and all that. aspects of multidisciplinary statistical mechanics, *Physics Reports* **254**, 215 (1995).
- [3] T. Kriecherbauer and J. Krug, A pedestrian’s view on interacting particle systems, KPZ universality and random matrices, *Journal of Physics A: Mathematical and Theoretical* **43**, 403001 (2010).
- [4] I. Corwin, The kardar-parisi-zhang equation and universality class, *Random Matrices: Theory and Applications* **1**, 1130001 (2012).
- [5] K. A. Takeuchi, An appetizer to modern developments on the kardar-parisi-zhang universality class, *Physica A: Statistical Mechanics and its Applications* **504**, 77 (2018).
- [6] M. Prähofer and H. Spohn, Universal distributions for growth processes in 1+1 dimensions and random matrices, *Physical Review Letters* **84**, 4882 (2000).
- [7] J. Baik and E. M. Rains, Limiting distributions for a polynuclear growth model with external sources, *Journal of Statistical Physics* **100**, 523 (2000).
- [8] K. Johansson, Shape fluctuations and random matrices, *Communications in Mathematical Physics* **209**, 437 (2000).
- [9] C. A. Tracy and H. Widom, Level-spacing distributions and the airy kernel, *Communications in Mathematical Physics* **159**, 151 (1994).
- [10] T. Sasamoto and H. Spohn, One-dimensional kardar-parisi-zhang equation: An exact solution and its universality, *Physical Review Letters* **104**, 230602 (2010).
- [11] G. Amir, I. Corwin, and J. Quastel, Probability distribution of the free energy of the continuum directed random polymer in 1+1 dimensions, *Communications on Pure and Applied Mathematics* **64**, 466 (2011).
- [12] C. A. Tracy and H. Widom, On orthogonal and symplectic matrix ensembles, *Communications in Mathematical Physics* **177**, 727 (1996).
- [13] T. Sasamoto and T. Imamura, Fluctuations of the one-dimensional polynuclear growth model in a half-space, *Journal of Statistical Physics* **115**, 749 (2004).
- [14] T. Imamura and T. Sasamoto, Fluctuations of the one-dimensional polynuclear growth model with external sources, *Nuclear Physics B* **699**, 503 (2004).
- [15] A. A. Saberi, H. Dashti-Naserabadi, and J. Krug, Competing universalities in kardar–parisi–zhang growth models, *Physical Review Letters* **122**, 040605 (2019).
- [16] M. Kardar, Replica bethe ansatz studies of two-dimensional interfaces with quenched random impurities, *Nuclear Physics B* **290**, 582 (1987).
- [17] J. M. Kim, A. J. Bray, and M. A. Moore, Zero-temperature directed polymers in a random potential, *Physical Review A* **44**, 2345 (1991).
- [18] <https://www.pks.mpg.de/asg2024>.